J. Space Weather Space Clim. 2022, **12**, 17

https://doi.org/10.1051/swsc/2022014

JSWSC

Available online at:
www.swsc-journal.org

RESEARCH ARTICLE OPEN ACCESS

The polarisation of auroral emissions: A tracer of the E region ionospheric currents

Léo Bosse[1,*], Jean Lilensten[1,6], Magnar G. Johnsen[2], Nicolas Gillet[3], Sylvain Rochat[1], Alain Delboulbé[1], Stephane Curaba[1], Yasunobu Ogawa[4], Philippe Derverchère[5], and Sébastien Vauclair[5]

[1] Institut de Plantologie et d'Astrophysique de Grenoble (IPAG) CNRS – UGA, 38400 Saint-Martin-d'Hères, France
[2] Tromsø Geophysical Observatory, UiT – The Arctic University of Norway, 9019 Tromsø, Norway
[3] Univ. Grenoble Alpes, Univ. Savoie Mont Blanc, CNRS, IRD, UGE, ISTerre, 38000 Grenoble, France
[4] National Institute of Polar Research, 190-8518 Tokyo, Japan
[5] DarkSkyLab, 31000 Toulouse, France
[6] Honorary Astronomer at Royal Observatory of Belgium, 1180 Brussels, Belgium

Received 7 June 2021 / Accepted 25 April 2022

Abstract – It is now established that auroral emissions as measured from the ground are polarised. The question of the information given by this polarisation is still to be explored. This article shows the results of a coordinated campaign between an optical polarimeter and several ground-based instruments, including magnetometers, the EISCAT VHF radar, and complementary luminance meters in the visible domain (Ninox). We show that in the E region, the polarisation is a potential indicator of the ionospheric currents, velocity, and dynamics.

Keywords: Aurora / Polarisation / EISCAT

1 Introduction

The main auroral emissions consist of the atomic oxygen and molecular nitrogen ion N_2^+. The former produces the red line (630 nm) at an altitude of about 220 km and the green line (557.7 nm) at around 110 km of altitude. The latter emits a large band among which the most prominent emissions are the blue (427.8 nm) and the purple (391.4 nm) around 110 km of altitude. Barthélémy et al. (2011) ran the first coordinated experiment between a polarimeter observing the red line and the EISCAT Svalbard Radar. The light polarisation may be defined by the Stokes parameters. Here, we use the measured parameters, namely the degree of linear polarisation (DoLP, in percent) and angle of linear polarisation (AoLP, in degrees). Barthélémy et al. (2011) concluded that the polarisation is due to collisions between precipitating electrons with characteristic energies of a few hundreds of electron volts, confirming experimentally the theoretical predictions by Bommier et al. (2011). Since then, it has been shown that not only the red line but actually the four above-mentioned auroral emissions are polarised when observed from the ground (Bosse et al., 2020). On the night between the 24th and 25th of February 2020, we ran a series of multi-instrument experiments using the EISCAT radar, a test optical device (Ninox, a low light luminance meter operating in the visible wavelengths[1]), and optical polarisation observations in clear weather conditions. We also benefited from observations from a chain of magnetometers.

The question that we aim to address is the following: do the polarisation properties of auroral emissions provide indications on the electromagnetic environment, and in particular on the currents in the ionosphere? The rationale behind this question is the link hypothetised by Duncan (1959) and Bommier et al. (2011) between the direction of an impacting electron flux and the auroral emissions which results from collisions with the upper atmosphere particles. The model of Bommier et al. (2011) predicts that a particle set in an energetic state by an impacting electron will emit a photon upon de-excitation with a polarisation depending on the direction of the incident electron. Thus, if a majority of electrons are moving in the same direction, we can expect the emitted light to be polarised. This global motion of electrons can be caused by a magnetic or an electric field. Previous studies (Bosse et al., 2020) have shown that the polarisation direction is not aligned with the magnetic field. Thus, if the polarisation is indeed produced at the emission, a revised physical model of the emission must be developed. The complex dynamical system that constitutes the

*Corresponding author: leo.bosse@univ-grenoble-alpes.fr

[1] https://darkskylab.com/english/index.html

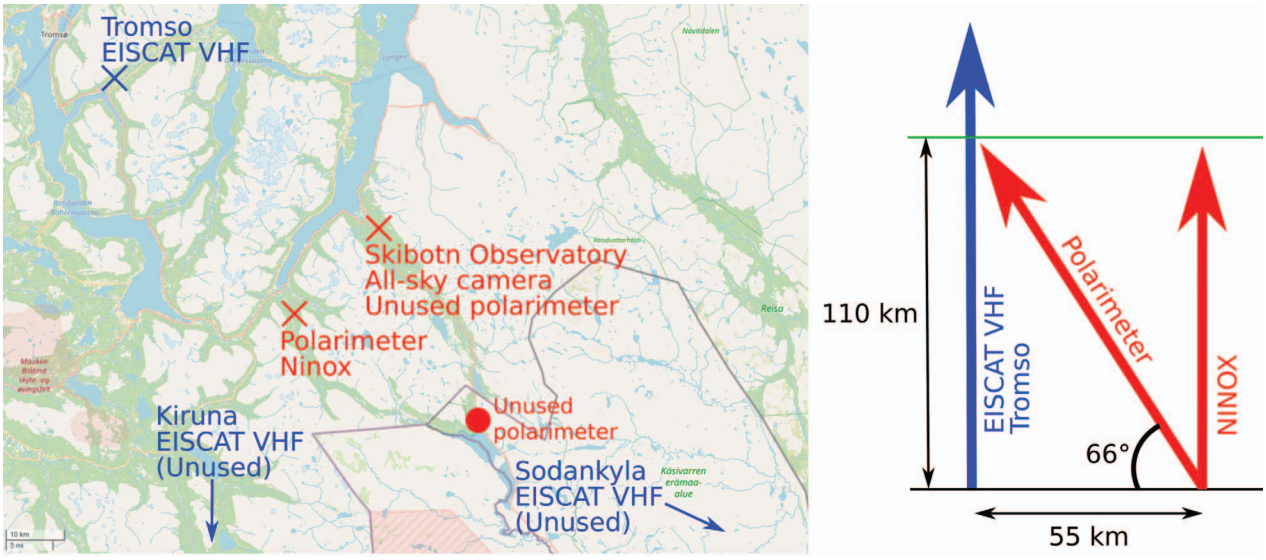

Fig. 1. Map and schematic representation of the experimental setup. Map credits: openstreetmap.

upper atmosphere, with highly variable Birkeland currents (aligned on magnetic field lines), Pedersen and Hall currents (horizontal), locally causes favored motion of charges. A current represents the differential motion of the charged particles with opposite charges. However, ionospheric currents are primarily carried by the motions of electrons (Kelley, 2009). To measure their 3D incoming direction is still out of reach for most instruments. It is, therefore, interesting to determine whether the polarisation of the auroral emissions could be an indicator of the direction of the electron flux.

The manuscript is organized as follows. In Section 2, we describe the experimental campaign. An intercomparison of measurements from several instruments is proposed in Section 4. Our main findings are summarized and discussed in Section 5.

2 Setting for the experimental campaign

We set up a dedicated one-week campaign with three polarimeters and the EISCAT radar from February 21st to 28th, 2020. The goals of this campaign were, therefore:

- To proceed to a tripole observation both with the 3 EISCAT VHF radar antennas and 3 distant polarimeters (see Fig. 1) to recover information on vector fields.
- To compare the polarisation in different emissions in order to possibly detect a vertical variability.
- To figure out whether this polarisation is produced in the ionosphere by comparing it with other indicators of ionospheric activity such as electron density, velocity measurements, and equivalent currents. And if this is the case;
  - To check whether or not the polarisation is correlated to the ion velocity.
  - To better understand the information contained in the DoLP and AoLP.

Unfortunately, we have been particularly unlucky with the weather. Out of the twenty radar hours and the 6 possible nights of observations, only one night (February 24–25, 2020) covering 6 radar hours met good meteorological conditions, and this only at one optical site, the closest to the EISCAT transmitting antenna located in Tromsø. Only one wavelength – the green one at 557.7 nm – could be observed. Nevertheless, we can start fulfilling several of our objectives through this single observation.

The global geophysical conditions were very quiet, with an adjusted solar $f_{10.7}$ index of 69 and an ap index ranging from 2 to 5 throughout the night. However, since we perform local observations, the global indices miss part of the information. We, therefore, rely on local magnetometer data (not shown) for geomagnetic activity monitoring and equivalent current computations.

2.1 EISCAT VHF

EISCAT VHF is an incoherent scatter radar whose main characteristics may be found in Lehtinen et al. (2002). The radar used here will be turned off in a few years to give way to the new powerful EISCAT_3D facility[2]. It operates at 224 MHz (VHF). The transmitter–receiver is located near Tromsø (19.2° E/69.6° N). It was pointing vertically, i.e., with an elevation of 90°. The two other antennas (in Kiruna and Sodankylä) were expected to point along the line of sight of the latter, but experimental failures prevented a successful coordinated campaign. The measurements are shown in Figure 2. We limited the upper altitude range to 400 km for the plot for the sake of clarity.

2.2 The polarimeter

The polarimeter used in this study has been fully described in Bosse et al. (2020). We, therefore, only recall here its basic principles. The auroral light is filtered through a narrow

[2] https://cloud.eiscat.se/index.php/s/XH2Y3mQeXat5wdW

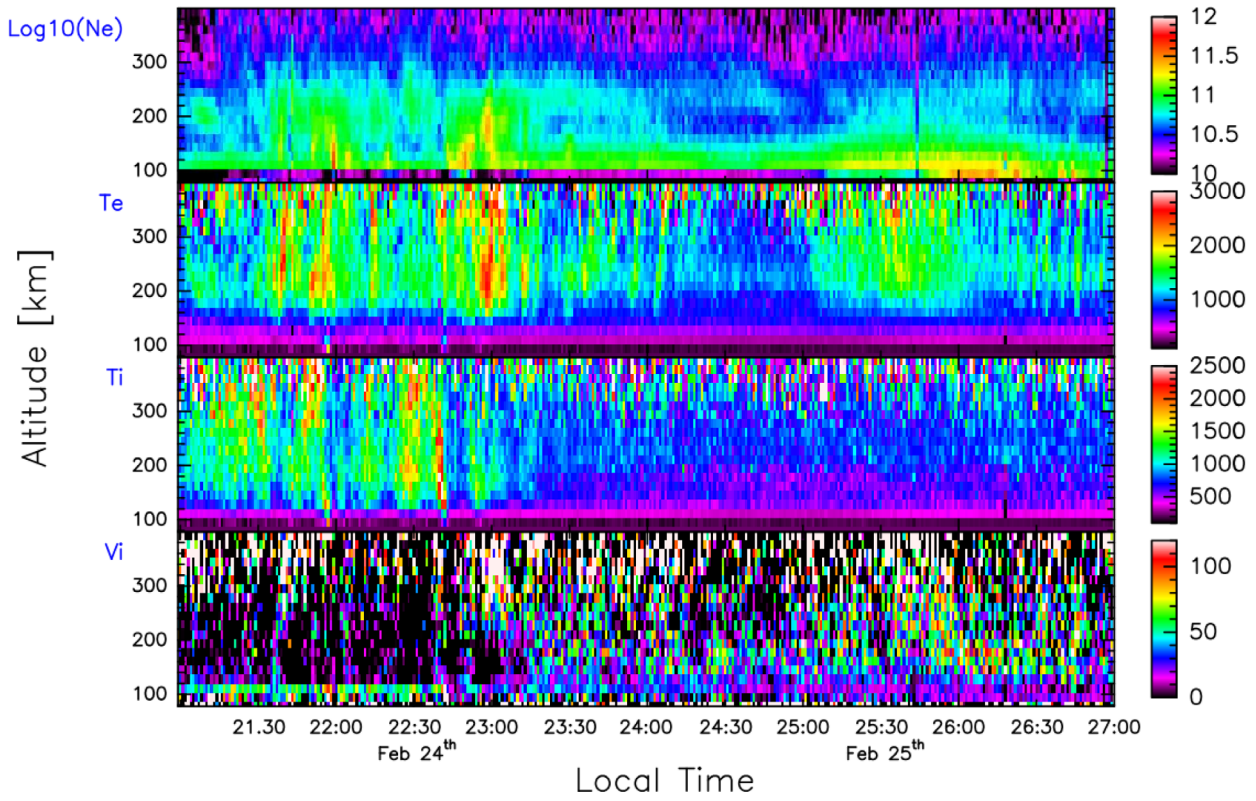

Fig. 2. EISCAT data. From top to bottom, the decimal logarithm of the electron density (in m^{-3}), electron temperature (in K), ion temperature (in K), and line of sight ion velocity (in $m.s^{-1}$). The time is local time, which is more readable than UT for local observations.

10 nm width optical filter centered around 557 nm. Immediately after, a polarising lens rotates at 2 Hz. The light is then transformed into a current through a photomultiplier and sampled at 1 kHz. A lock-in analysis is performed in real-time. This powerful method allows a fast and accurate computation of the polarisation via the DoLP and AoLP. A DoLP of 100% corresponds to a fully polarised light. By convention, an AoLP of 0° corresponds to a vertical polarisation and is π-periodic. When the radiant flux and the DoLP become too small, the AoLP can hardly be computed and becomes very erratic. To avoid this problem, all data presented in this study are smoothed over a sliding window of 20 s. The objective of the smoothing process is to reduce the measurement errors and, in particular, lower the potential over-estimation of the DoLP due to measurement noise and obtain a clearer AoLP behavior (see Appendix A). This instrument has been calibrated both in DoLP and AoLP. This sliding average is necessary to analyze the data at the expense of smoothing out rapid variations. It constitutes a trade-off between a high signal-to-noise ratio and a short time resolution. As the observation spans several hours and the main point of the article concerns changes on time scales much longer than the sampling period, losing the details on time scales below 20 s is acceptable. The polarimeter was installed on the top of a small mountain pass at 69.223° N latitude and 19.981° E longitude, 55 km away from the radar. The orientation of the polarimeter is such that its line of sight crosses that of the radar at 110 km altitude, where the green line is emitted. The polarimeter was thus measuring at an elevation of 66°, and with an azimuth of −37° (i.e., towards North–West).

The data are shown in Figure 3. The top panel shows the radiant flux measured by the instrument. This radiant flux is not calibrated and is given here in arbitrary units (a voltage in mV measured by the polarimeter). The DoLP and the AoLP are shown in the middle and bottom panel, respectively. The DoLP is given in percent, and the AoLP in degrees with respect to the vertical.

2.3 The equivalent currents

Based on ground-based magnetometer data from multiple sites, and in particular the observed magnetic field variations, it is possible to solve an inverse problem in order to obtain associated equivalent currents flowing above the measurement sites. These currents are called "equivalent currents" since they do not necessarily represent the real current system but an (equivalent) system that generates the same magnetic field variations. Possibly the most common approach for this is the spherical elementary current system (SECS) technique introduced by Amm (1997) and Amm & Viljanen (1999). Assuming a 2D current sheet of infinitesimal thickness in the auroral E-layer (~110 km), the equivalent currents can be established from the magnetic field measurements. The current sheet will then consist of a series of superposed divergence-free currents (vortex-like elementary currents) centered on a set of poles. Singular value decomposition is the method normally used to solve the inverse problem. The method requires a cut-off point for small singular values, which is determined by the so-called ϵ parameter. In practice ϵ determines the scale length of the spatial

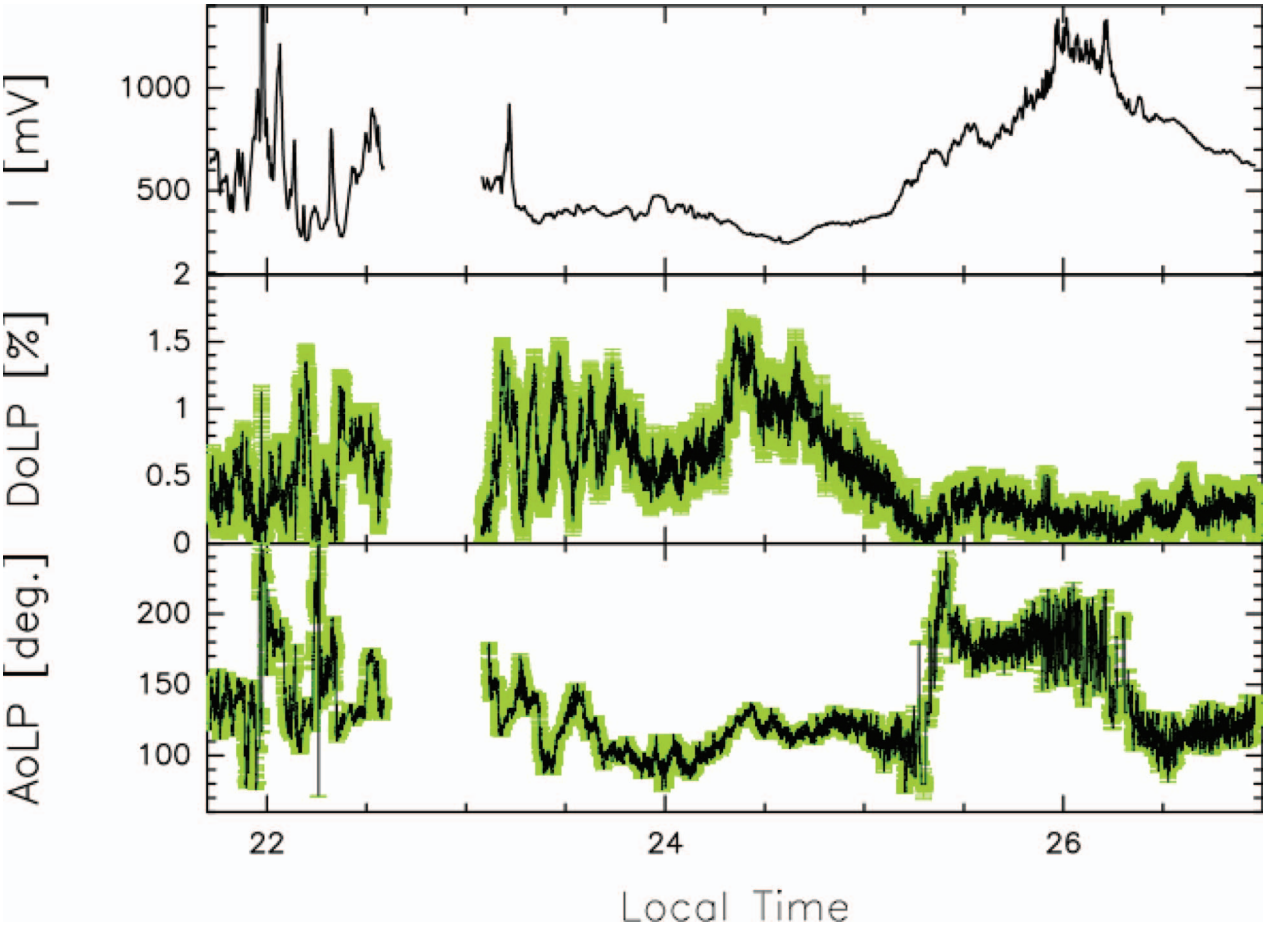

Fig. 3. Polarimeter data for the green line (557.7 nm) averaged over 20 s (see Appendix A). From top to bottom, the radiant flux is measured in mV, the Degree of Linear Polarisation (DoLP), and the Angle of Linear Polarisation (AoLP). The error bars are in green, and the values in black. For the sake of clarity, only AoLPs corresponding to DoLPs larger than 0.15% has been plotted.

variations in the solution; small values lead to unrealistic small scale features and vortexes, while large values effectively low pass filter the end result. For further details and discussion about the SECS methodology, see e.g., Vanhamäki & Juusola (2020) and references therein.

Ideally, in order to achieve the best results with the SECS technique, an evenly distributed and dense grid of magnetometer stations is needed. However, in practice, this is never the case. For example, in the high latitude European sector, the distribution of land and sea severely limits where it is possible to deploy magnetometers. In the analysis of results generated by the SECS technique one needs to take care not to over-exaggerate which conclusions can be drawn. Generally, it is safe to assume that the solution gives a more realistic result between stations than towards the outskirts of the area of study, where the inverse problem will be more ill-posed.

In the present study, we have used $\epsilon = 0.05$. This number was found by testing different values on a known current above the IMAGE network of magnetometers (Tanskanen, 2009) – the network used in our study – in a similar fashion as suggested by Weygand et al. (2011). The model current used was generated with the Python package pyAMPS (Laundal et al., 2018). Figure 4 shows a map with the calculated equivalent currents above Fennoscandia. Note that the unit is A km^{-1}. Indeed, since we are assuming that the current sheet is infinitesimal and flowing on a shell 110 km above ground, we are dealing with a height-integrated current. The current density of a 3D current would be A km^{-2}, after integrating it in one direction (here the height), we end up with A km^{-1}. In order to keep this particularity in mind, we will refer to the "height integrated current" in the following, although the integrating layer is considered infinitely thin. Figure 5 displays the Eastward and Northward components of the height integrated current above Tromsø.

2.4 The Ninox

In order to check the state of the sky, we rely on the data from the National Norwegian meteorological service and from all-sky cameras located in Skibotn. However, these measurements again miss information. If most of the sky was cloudy, one site among the three kept a clear sky during all the experiments. Indeed, they do not provide the local state of cloud coverage at each three observation sites. The all-sky camera is only present at the Skibotn observatory, and the meteorological service is not precise enough. We also took an optical

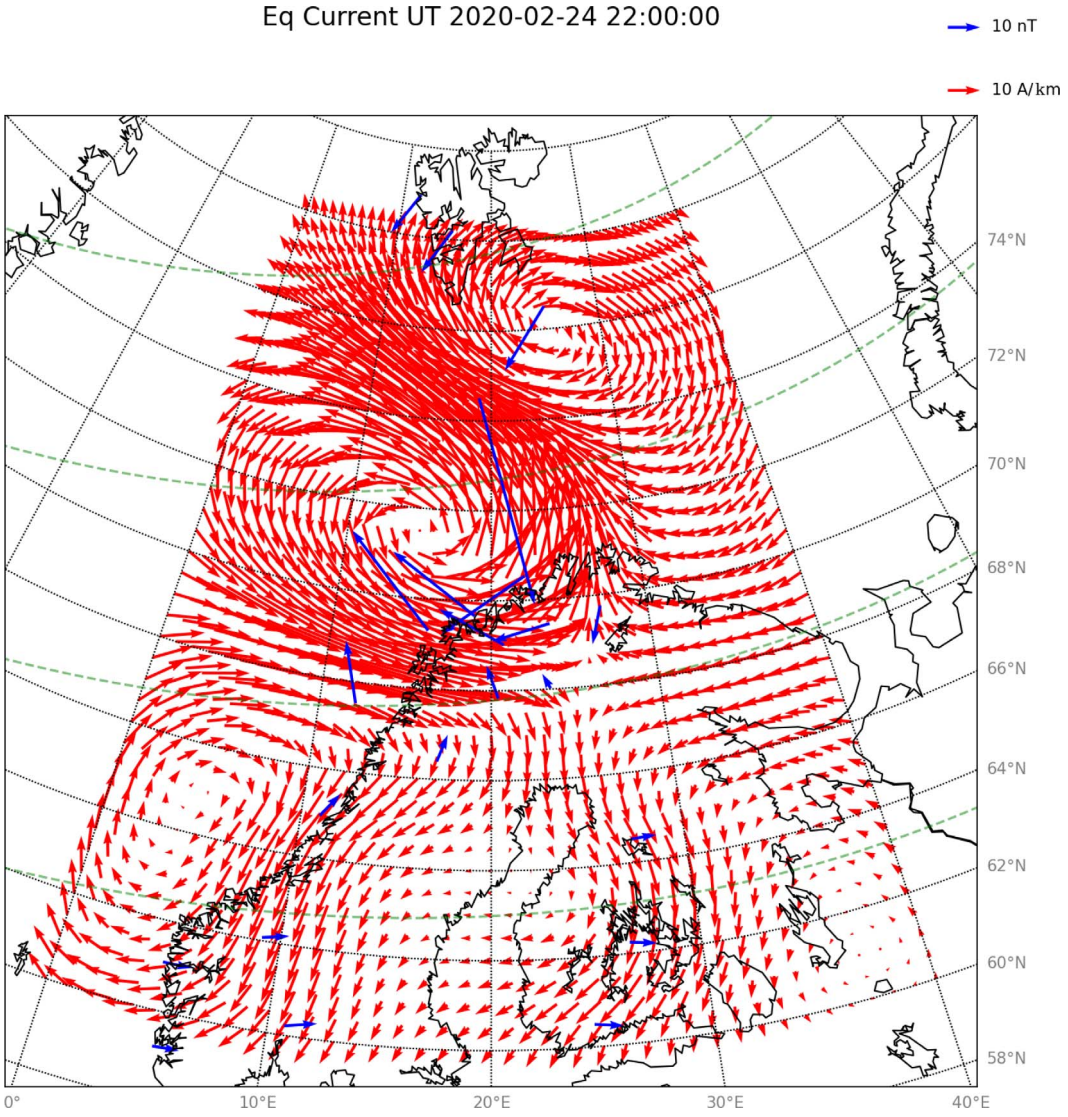

Fig. 4. Map showing estimated equivalent currents (red arrows) above northern Fennoscandia on February 24. 21.23 UT / 22.23 LT. Accompanying magnetic field disturbances measured at the IMAGE magnetometer stations and used as input to the SECS method are indicated with blue arrows.

instrument called Ninox to measure the sky brightness at the zenith every minute during the observing session. We show the Ninox measurements in detail in Appendix B. It tends to show that the sky was clear during the observation and that the light pollution from nearby cities did not vary abruptly throughout the night. With the presence of the auroral emission, the Ninox could not allow us to detect a smooth change of the light pollution level over several hours, but it could clearly show a sudden extinction of a municipality's public lighting, for instance.

3 Description of the observations

3.1 EISCAT data

In Figure 2, the electron density is a good indicator of geophysical activity. At the beginning of the night, the electron density is enhanced mainly in the F region, typically above 150 km height. The precipitation occurs all along the night, with enhancements of their energy before 23:30 LT and after 25:00 LT that create an increase of the electron density at a lower altitude, down to 90 km. We will mostly discuss the latter in the following, as polarimeter data are not accessible around 23:00 (see below). The electron temperature at 110 km – where the green line is emitted – is classically equal to the ion temperature because collisions at this altitude equalize all the temperatures (including that of the neutrals). However, one sees an enhancement of the electron temperature at high altitude, corresponding to soft electron precipitation. The ion velocity is positive away from the radar. It is harder to further interpret a 3D plot. Detailed data will be shown at the altitude of the green line emission in the following paragraphs. It should be noted that since the measurement is not field-aligned, sharp boundaries, such as that seen at 100 km in the electron

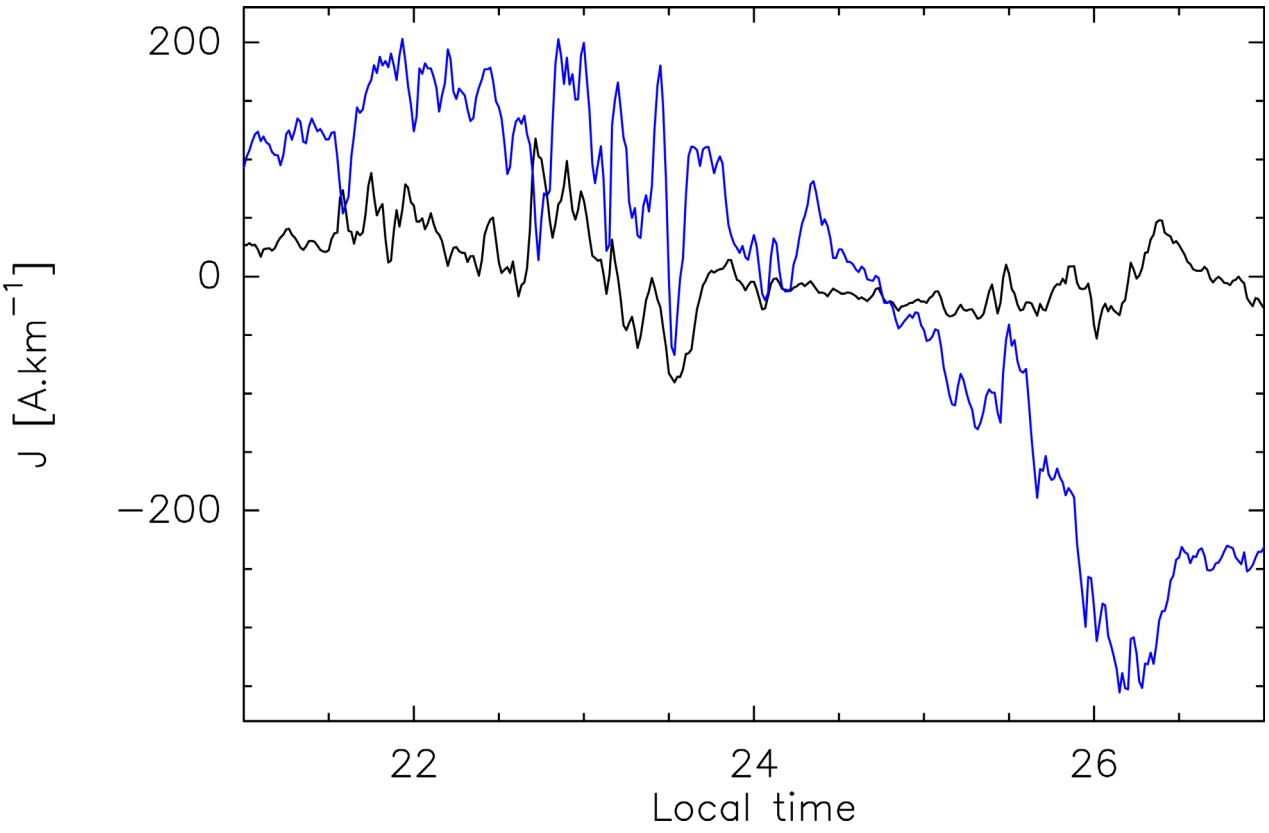

Fig. 5. Height integrated currents above Tromsø EISCAT antenna deduced from the magnetometers. The northward component is in black and the eastward in blue.

density, might be due to the contributions from different magnetic lines.

3.2 Polarimeter data

At the beginning of the observation period (see Fig. 3), a series of auroras occur in the line of sight, as the radiant flux is more than doubling on a short time scale. From about 22:30 to 23:00 LT, the gap in the data is associated with a series of calibrations. The night gets quieter around midnight before an enhancement of the green line radiant flux, simultaneous to the event seen in the EISCAT observations.

Interestingly, the DoLP decreases with increasing radiant flux in the second part of the observation (the DoLP decreases by a factor of ~5, while the radiant flux is enhanced by approximately the same factor). Similar behavior was already observed with the red line polarisation (Lilensten et al., 2013). This anticorrelation between the DoLP and the radiant flux is still not understood. Lilensten et al. (2015) interpret it as an effect of depolarising collisions. However, the DoLP does not drop completely to zero and still allows for the study of the polarisation. The AoLP exhibits a very spectacular feature, though. Between about 25:10 and 26:20 LT, it rotates by about 70°. When subtracting 70° to the AoLP during this short period, the angle appears continuous (see later, Fig. 7). Note that at the start and end of the jump, the DoLP is too low to allow for any interpretation of the AoLP. It is clear when looking at the AoLP error bars spanning 180°. However, in between this period, the DoLP increases enough to allow an interpretation of the AoLP, as explained in Appendix A.

3.3 Equivalent current model

In the center of Figure 4 we observe a strong eastward height integrated current above northern Norway, which rotates northwards further east and north. This is a classic picture of the Harang discontinuity.

In Figure 5 the crossing of the discontinuity, e.g., rotation from eastward to westward height integrated current, occurred at around 25 LT. Assuming that the equivalent height integrated currents as calculated by the SECS method are close to real height integrated currents and that the disturbances on the ground in the auroral zone are mainly due to Hall currents, the direction of the height integrated current is also an indicator of the (negative) $E \times B$ motion of electrons in the E-layer.

4 Inter-comparison of the several measurements

4.1 Polarimeter versus EISCAT

4.1.1 Green line radiant flux versus electron density

Let us concentrate first on the comparison between the electron density and the green line radiant flux displayed in Figure 6.

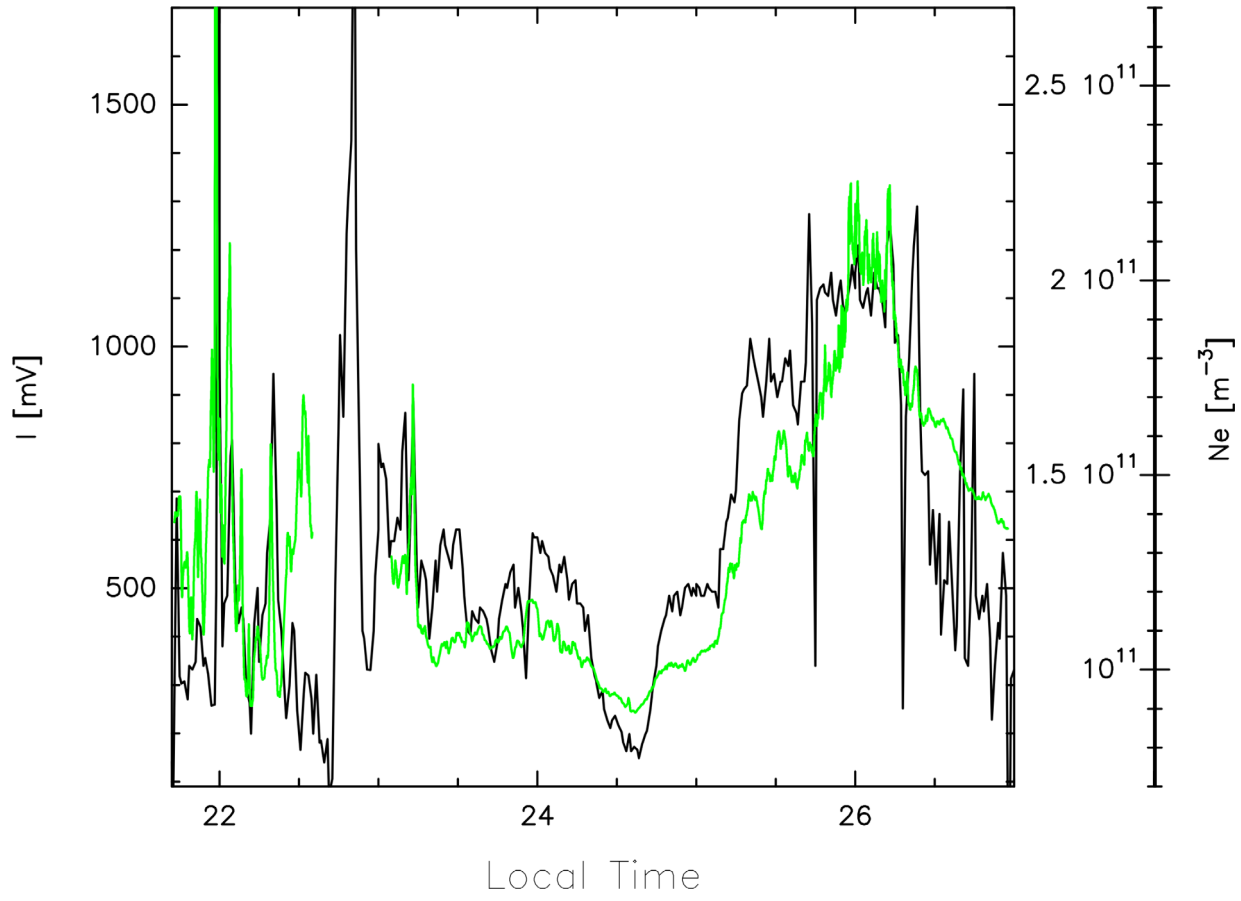

Fig. 6. This figure compares the EISCAT data at 110 km from Figure 2 (black line) to the green line polarimeter radiant flux as in Figure 3 (green line).

Since the green line maximizes at 110 km, we plotted the EISCAT data at this altitude. However, for comparison, the electron density measurements at 100 and 120 km will be shown later as well. Care must be taken on the fact that the units are different (mV vs. m^{-3}), and therefore, only the trend can be significant. The radiant flux and the electron density at 110 km evolve with similar dynamics, confirming the altitude of the emission to correspond to the maximum emission of the auroral green line. The variability of the two observables – radiant flux and electron density – is close, although they do not overlap at the beginning of the night with this scale. From this comparison, we can assess that radiant flux variations observed in the green line originate in the upper atmosphere. Indeed, both the electron density enhancement and the neutral atomic oxygen emission are effects of the electron precipitation. Since EISCAT does not depend on the cloud cover, we can also exclude that the optical observations are an effect of a reflection of distant city lights on the clouds: should one have clouds, the green line would have had no reason to follow the electron density, which is well above the cloud coverage. This conclusion is supported by the Ninox data presented in Appendix B. However, we can not exclude a constant contribution from light pollution. This contribution is not at the origin of the variations and is expected to be almost stationary over the whole observation.

4.1.2 Green line polarisation parameters versus electron density and ion velocity

Figure 7 (top panel) compares the green line radiant flux and the electron density at 3 altitudes (100, 110, and 120 km). Here again, we compare parameters with different units. Therefore, only the dynamics should be considered and not the absolute values. Until about 24:30 LT, the electron density decreases at all altitudes, followed by a fast increase until 26 LT. The ionosphere empties again gradually in the last hour of observation. This behaviour corresponds closely to that of the green line radiant flux, especially at 110 km.

Figure 7 (bottom panel) compares the AoLP and the ion velocity measured by EISCAT at 100, 110, and 120 km. We search here for a correlation between the observed AoLP and a tracer of the ionospheric current at the emission. As we do not have direct access to the current orientation, we assume that variations of the current orientation are reflected in its magnitude and thus on the ion velocity as measured by EISCAT. Before 23:00, the AoLP and the ion velocity are very dynamic, with sudden increases over a few minutes. After the gap in the data, their behaviour is more stable. The behaviour of the ion velocity and that of the AoLP look similar at 110 and 100 km (keeping in mind that we compare only the dynamics, as the units are different, mV against m/s), except for the period

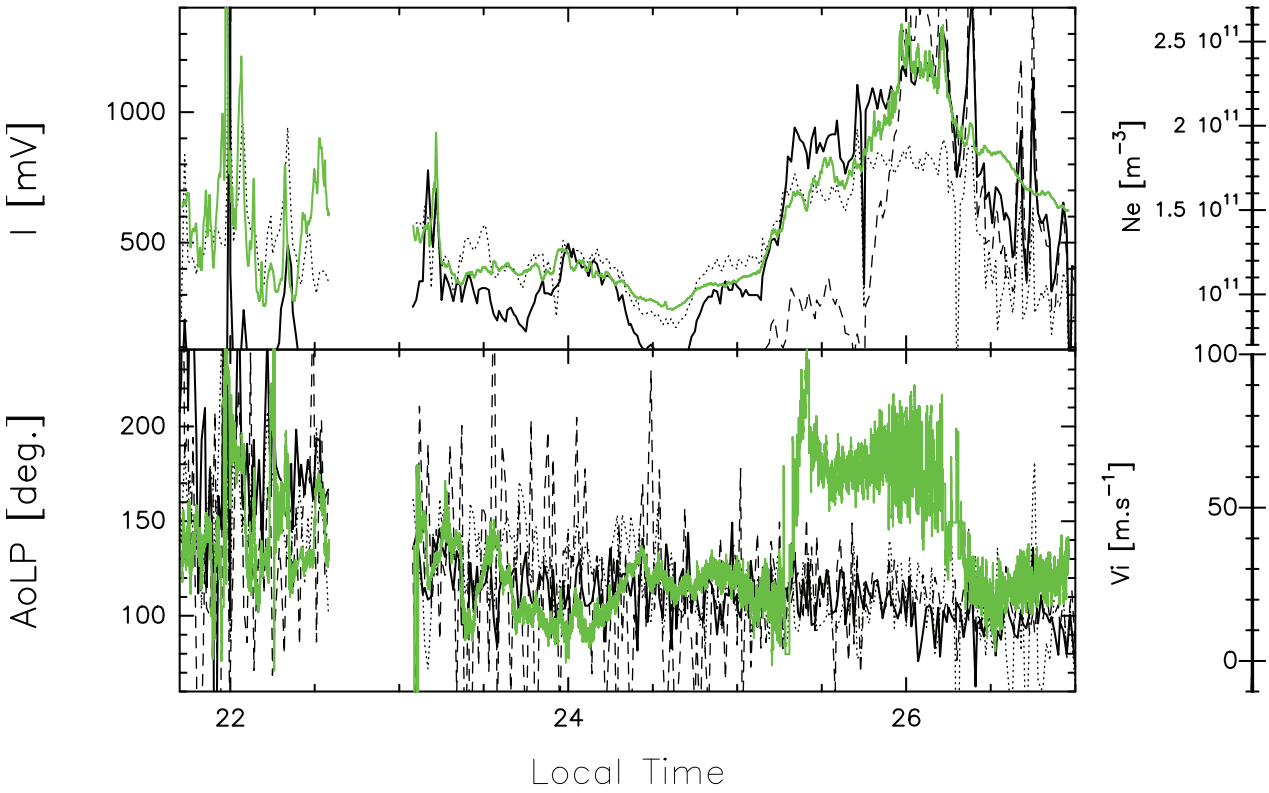

Fig. 7. The polarimetric data from Figure 3 are shown here in green. We took off the error bars for the sake of clarity. In black, the EISCAT data at 100 km (thin dashed line), 110 km (heavy full line), and 120 km (thin dotted line) from Figure 2: top panel shows the electron density and bottom the ion velocity. Vi is positive away from the radar. For the sake of clarity, only AoLPs corresponding to DoLPs larger than 0.15% has been plotted.

from 25:10 to 26:20 LT that shows a large shift between the two parameters. This shift is about 70°. This number is, of course, indicative, as values ranging between −60° and −90° would partly reconcile the continuity in the observed angle. It is not an instrumental artifact and, therefore, must indicate a physical phenomenon, for which we provide a tentative explanation later on.

4.2 Polarimeter versus magnetogram and ionospheric currents

As explained in Section 2.3, it is possible with some approximation to extract the horizontal ionospheric height integrated current from the chain of magnetometers (mainly Hall current). Using the same geometry as for the AoLP, we deduce the apparent angle of the current projected on the polarimeter (noted AoJ). The apparent angle of the equivalent height integrated current corresponds to its projection on the detector, measured as an angle that matches the measure of the AoLP. For the detailed computation, we refer to the Appendix of Bosse et al. (2020). In Figure 8, we compare the horizontal height integrated current intensity (i.e., $\sqrt{J^2_{\text{east}} + J^2_{\text{north}}}$) to the green line radiant flux and the AoLP to the AoJ.

The agreement between the total height integrated current and the radiant flux of the green line is particularly clear. Here again, subtracting 70° to the AoLP during the jump phase around 25:00, reconciles the AoLP and the AoJ. To a lesser extent, the same agreement can be seen in the comparison between the AoLP and the AoJ (once shifted for the 70° jump around 25:00 as discussed below). Not only do the two series show strong similarities, but also the amplitude of the AoJ and the AoLP are close to one another. This is particularly evident in the stable periods (the first and last parts of the experiments) but still visible in the middle of the night. These similarities, along with the comparison with the EISCAT electron density, are again a severe hint that the polarisation occurs, at least partially, in the upper atmosphere and not during its path through the atmosphere or by Rayleigh diffusion. It is probably audacious to conclude from this single comparison that the AoLP is a tracer of the currents, but this is, however, a solid hint on the path to explain the polarisation behaviour.

There are some differences. though. These differences may originate in different sources: electron precipitation along the magnetic field lines, but also the fact that the green line does not only originate through electron impact collisions with the atomic oxygen (see Sect. 5) and that these other sources are isotropic and therefore not a candidate to create a polarised emission. Following the first point (electron precipitation along the magnetic field lines), this motion would add up to the horizontal motion along with the equivalent current and create a total current with a vertical component. Thus, the apparent angle of this resulting current will differ from that of the equivalent current angle, which may explain the observed difference.

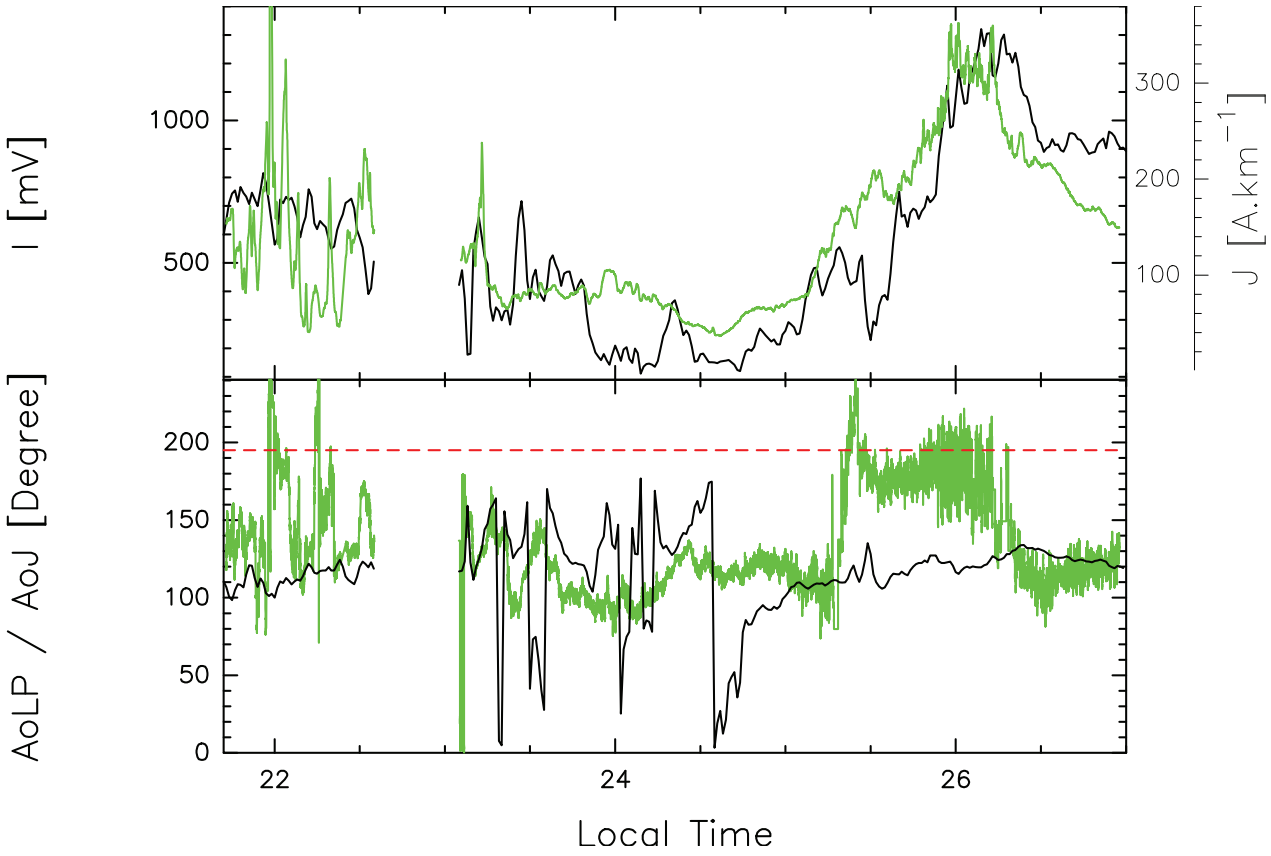

Fig. 8. The green line radiant flux (top) and its AoLP (bottom) from Figure 3 are shown in green. We took off the error bars for the sake of clarity. In black, the full line represents (top) the total height integrated current deduced from the magnetometer chain and (bottom) its apparent angle projected on the polarimeter. It is noticeable that the scales are the same for the AoLP and the apparent current angle. The red dashed line represents the apparent angle of the magnetic field at 110 km (which is 195°). For the sake of clarity, only AoLPs corresponding to DoLPs larger than 0.15% has been plotted.

Such a model based on the polarisation measurements and the equivalent current computation could help monitor the 3D ionospheric current system in the future.

In Figure 8, we also show the apparent angle of the magnetic field at 110 km as seen from the polarimeter, i.e., 195°. A questioning feature is that during the short period when the AoLP jumps by 70°, it gets almost aligned to the magnetic field. However, as for above, one must remain careful in not over-interpreting such a short period of time.

5 Discussion and conclusion

5.1 Where does the jump in the AoLP originate?

Although this set of observations only spans over 6 h, we believe it is important to explore the physics that could help interpret the jump in the AoLP around 25:00. We maintain that this is not an instrumental artifact and must correspond to a geophysical process. The facts are that between about 25:10 LT and 26:20 LT, the AoLP rotates by a value of about 70°. The exact value is subject to caution (ranges between 60° and 90°, and may even evolve during this period). With such a short period of time, developing sophisticated mathematics to refine it seems improper. When we subtract this 70° value to the AoLP, the dynamics of the AoLP become comparable to that of the ion velocity at 110 km, while the AoLP value approaches the apparent angle of the height integrated current (AoJ).

The first possibility to investigate is the interaction between the scattering of light pollution and auroral light. It is reasonable to consider light pollution to be roughly constant throughout the night. It is thus unlikely that this process can account for the observed 70° jump. However, changes in the relative contributions from light pollution and auroral lights could induce such observed polarisation variations. For example, if light pollution is the dominant source of polarisation during quiet auroral activity, the period of the jump may correspond to a bright auroral arc in the line of sight that would take over, significantly affecting the polarisation. It is likely that both contributions are always mixed in varying proportions. At the start and end of the AoLP jump, both contributions would be approximately evenly mixed, and thus the DoLP would drop down to zero while the AoLP would be close to being undefined, as is observed in our case. Another factor that can induce polarisation variations in light pollution scattering is the presence of low altitude aerosols (dust, ice crystals, droplets…). One of their effects is to scatter the light in the atmosphere, creating a specific polarisation in a favored direction through Rayleigh and/or

Mie scattering (van de Hulst, 1981; Born & Wolf, 1999). Depending on their cross-section and composition, they can produce polarisation in any direction, thus shifting the observed AoLP up to 90° (Ugolnikov et al., 2004). Their study requires the modeling of a single or multiple scattering approach, which is out of the scope of the present article. It should take into account a wide range of input parameters, such as the complex refractive index, the aerosol sizes, and their vertical profiles (Dubovik et al., 2000). In the present situation, this scenario seems unlikely but cannot be excluded. Although the multi-instrument approach detailed above shows that the polarisation parameters are closely linked with the upper atmosphere behaviour, including during this AoLP jump, we cannot exclude that the emitted polarisation angle is transformed by the aerosols.

Another possibility deals with the energy of the impacting electrons. Bommier et al. (2011) studied the theoretical polarisation of the O I 630 nm red line in the aurorae. Through a semi-classical formalism for collisional transition, they show that the AoLP depends on the energy of the impacting electrons. The energy threshold of the red line is 1.96 eV. When the electron energy is close to the threshold (typically smaller than 2.0 eV), the angle of polarisation is oriented at 90° with respect to the incident direction of the electrons. Above typically 2.4 eV, it is aligned with the incident direction. It can then rotate when switching between these two energy values. Care must be taken, though. This theoretical study is valid for a quadrupolar electric line that does not stand for the green line. However, the experimental green line observations resemble the predictions by Bommier et al. (2011) for the red one. This must be confirmed by further modeling and experiments. If confirmed, the AoLP would become a direct measurement of the energy range of the impacting electrons.

Finally, this could be an indication that during this short period, the main currents become mainly field-aligned and not mainly horizontal anymore. This interpretation is supported by the comparison between the AoJ deduced from the magnetometers and the AoLP in Figure 8. By construction, the AoJ reconstructed from the magnetometers cannot capture the vertical currents. The agreement between the AoLP and the AoJ outside the jump period tends to confirm that we face horizontal currents (mainly Hall currents). During the jump phase, the AoLP becomes close to the apparent angle of the magnetic field lines (the inclination of the magnetic field at 110 km is 78.4° as estimated from the IGRF-12 model; Thébault et al., 2015). This behaviour could be a sign that the field-aligned current was dominant during this time period. In the absence of more observations, one must remain careful though and take this as a motivation for more experiments and modeling. If confirmed, a joint interpretation of magnetometer and polarimeter data may help determine the 3D ionospheric currents.

5.2 Main results

In setting this experiment campaign, we had several goals that can be summarized as follows. One was to observe the polarisation at different altitudes (i.e., emission lines) from different places in order to retrieve 3D parameters. One was to determine where the polarisation occurs, either at or in the vicinity of the emission, during the travel of photons to the ground instrument, or because of Rayleigh and/or Mie scattering due to sources out of sight. Another one was to see whether the AoLP follows the direction of the ions and could be used as a measurement for the currents at different altitudes.

The meteorological conditions prevented us from fulfilling the first objective, and we were left with only one night at only one wavelength, the green line at 557.7 nm. In this set of hours, the similarity between the dynamics of the radiant flux of the green line and that of the electron density at 110 km height is not surprising but gives a good indication that the emissions observed come from the same observation volume for the 2 instruments and not from an aurora occurring elsewhere in the sky and being reflected in the polarimeter through scattering in the lower atmosphere. Fortunately, we could compare the behaviour of the ion velocity measured by EISCAT to that of the AoLP measured by the polarimeter showing an agreement between the two. Again, there are at least two possibilities for the polarisation to occur. The first one is through scattering from auroras occurring elsewhere in the sky. That is possible and may constitute an additional source. It is under study but necessitates the development of a dedicated radiative transfer model. The second source is a polarisation at the origin of the emission due to the fact that the impacting particles are focused. Considering Figure 7, it seems to be the case. This would have several important consequences:

- The green line is due to the deactivation of the O^1S oxygen state relaxing on O^1D (with a branching ratio of 0.94) with a companion UV emissions at 297.6 nm (6%). It is supposed not to be polarisable from quantum mechanics models (Bommier et al., 2011) since its upper state (1S) is not degenerate. The energy threshold is 4 eV. However, the origin of this excited state is still unclear for airglow emissions: Gronoff et al. (2008) have shown that the current belief of a three-body collision (Barth mechanism, see Barth & Hildebrandt, 1961) is not sustainable when compared to the potential energy curves of the oxygen atom. Should this three-body collision be valid, it would be fully isotropic. Therefore, this emission line should not be polarised. Our observations may indicate that the polarisation of the electromagnetic emission is not created at the emission itself but during the crossing of the charged medium through a mechanism still to be modeled. Should the green line be polarised at the $O^1S \rightarrow O^1D$ de-excitation, would then (i) definitely rule out the Barth mechanism and (ii) oblige to reconsider the model of the atomic oxygen.
- The green line originates in the spontaneous radiative de-excitation of the O^1S state. The sources to excite the oxygen in this state are listed in Witasse et al. (1999). They include the electron impact, the collisional deactivation of the $N_2(A^3\Sigma_u^+)$ state, the dissociative recombination of O_2^+ colliding with thermal electrons, and chemical reactions. During the day, the photodissociation is, of course, a supplementary source. For auroral emissions, the electron impact is considered the only non-isotropic source and thus the only source of polarised emissions. These electrons are precipitating along the magnetic field line. Therefore in Lilensten et al. (2013), we claimed that the AoLP was a good tracer of the magnetic field line. We had neglected the fact that the electrons do not only move along the magnetic field in the ionosphere but also have a horizontal motion along with current systems. Considering the

magnetic field only, we had claimed that the best measurement was perpendicular to the magnetic field line. This may be the case in the F region, where the Birkeland currents are mostly aligned along the magnetic field. In the E region, the Hall and Pedersen conductivities create horizontal currents that close the system at its bottom. The precipitations along the magnetic field lines are always present and are part of the physics behind the polarisation. The comparison between the ion velocity measured by EISCAT and the AoLP (Fig. 7) is a good marker for this. But these field-aligned precipitation cannot explain everything. Indeed, the AoLP has the same amplitude and same behaviour as the apparent angle of the horizontal current (AoJ). The differences between the two may be explained by the currents flowing along the magnetic field lines. If this proves to be correct (through more multi-instruments experiments), future coordinated observations between a chain of magnetometers and a chain of polarimeters may allow retrieving the 3D currents in the ionosphere. Other excitation mechanisms could also be considered as non-isotropic and the source of polarised emissions. In this case, the varying relative contribution of different mechanisms could explain the observed polarisation variations. In this case, the identification of the processes at play adds complexity to the interpretation of the polarisation data but could offer a new way to monitor the upper atmosphere.

There are still many questions to answer. Among them:

- We have shown in Bosse et al. (2020) that the nitrogen purple and blue lines are also polarised, after having shown in different papers already cited that the red line is. Does their AoLP also witness electrical currents?
- What does the DoLP tell about the upper atmosphere? In this work, we could not find a clear pattern, although it seems to obey the fluctuation of the magnetic field intensity and to be correlated to the AoLP.
- What is the role of scattering? Could an auroral emission outside the field of view create at least part of the observed polarisation through Rayleigh and/or Mie scattering?
- In this context, what is the role of the aerosols? Could they explain, at least partially, our observations?

Our results need to be confirmed by more observations. However, campaigns involving a large group with many instruments are difficult to set up. Thus, we might need to rely only on our already acquired set of data for some time. The most important future step is, therefore, to put efforts into the modeling by solving the radiative transfer equation in order to understand better the physics behind these observations and to discriminate between the several sources at play (vertical precipitation, horizontal currents, aerosols, etc.).

Acknowledgements. This work was partially funded by the IPEV project on the high latitude polarisation of the auroral emissions POLARLIS (project number 1026). It was also funded by the Prematuration CNRS program and by the Maturation program CM180023, project PTCU number 180018M from the SATT company Linksium. This work was supported by the Programme National PNST of CNRS/INSU co-funded by CNES and CEA. The polarimeter is patented by CNRS and valorised by Linksium (international patent number 1873378). The results presented in this paper rely on geomagnetic indices calculated and made available by ISGI Collaborating Institutes from data collected at magnetic observatories. We thank the involved national institutes, the INTERMAGNET network, and ISGI (http://isgi.unistra.fr). We are very grateful to the EISCAT board who selected our proposal for the invited science program PP. EISCAT is an international association supported by research organisations in China (CRIRP), Finland (SA), Japan (NIPR and ISEE), Norway (NFR), Sweden (VR), and the United Kingdom (UKRI). We thank the institutes who maintain the IMAGE Magnetometer Array: Tromsø¸ Geophysical Observatory of UiT the Arctic University of Norway (Norway), Finnish Meteorological Institute (Finland), Institute of Geophysics Polish Academy of Sciences (Poland), GFZ German Research Centre for Geosciences (Germany), Geological Survey of Sweden (Sweden), Swedish Institute of Space Physics (Sweden), Sodankylä Geophysical Observatory of the University of Oulu (Finland), and Polar Geophysical Institute (Russia). The editor thanks Masada Tzabari and an anonymous reviewer for their assistance in evaluating this paper.

References

Amm O. 1997. Ionospheric elementary current systems in spherical coordinates and their application. *J Geomagn Geoelectr* **49(7)**: 947–955. https://doi.org/10.5636/jgg.49.947.

Amm O, Viljanen A. 1999. Ionospheric disturbance magnetic field continuation from the ground to the ionosphere using spherical elementary current systems. *Earth Planets Space* **51**: 431. https://doi.org/10.1186/BF03352247.

Barth CA, Hildebrandt AF. 1961. The 5577 A airglow emission mechanism. *J Geophys Res* **66(3)**: 985–986. https://doi.org/10.1029/JZ066i003p00985.

Barthélémy M, Lilensten J, Pitout F, Simon Wedlund C, Thissen R, et al. 2011. Polarisation in the auroral red line during coordinated EISCAT svalbard radar/optical experiments. *Ann Geophys* **29(6)**: 1101–1112. https://doi.org/10.5194/angeo-29-1101-2011.

Bommier V, Sahal-Brechot S, Dubau J, Cornille M. 2011. The theoretical impact polarisation of the O I 6300 Å red line of Earth Auroræ. *Ann Geophys* **29**: 71–79. https://doi.org/10.5194/angeo-29-71-2011.

Born M, Wolf E. 1999. *Principles of optics: Electromagnetic theory of propagation, interference and diffraction of light*, Cambridge University Press, Cambridge. ISBN 9781139644181.

Bosse L, Lilensten J, Gillet N, Rochat S, Delboulbé A, et al. 2020. On the nightglow polarisation for space weather exploration. *J Space Weather Space Clim* **10**: 35. https://doi.org/10.1051/swsc/2020036.

Dubovik O, Smirnov A, Holben BN, King MD, Kaufman YJ, Eck TF, Slutsker I. 2000. Accuracy assessments of aerosol optical properties retrieved from aerosol robotic network (AERONET) sun and sky radiance measurements. *J Geophys Res: Atmos* **105(D8)**: 9791–9806. https://doi.org/10.1029/2000JD900040.

Duncan R. 1959. Polarization of the red oxygen auroral line. *Planet Space Sci* **1(2)**: 112–IN3. https://doi.org/10.1016/0032-0633(59)90006-6.

Gronoff G, Lilensten J, Simon C, Barthélemy M, Leblanc F, Dutuit O. 2008. Modelling the Venusian airglow. *A&A* **482(3)**: 1015–1029. https://doi.org/10.1051/0004-6361:20077503.

Kelley M. 2009. The Earth's ionosphere. In: *Plasma physics and electrodynamics*, Vol. **96** of International Geophysics Series, Elsevier Academic, Cambridge, MA. ISBN 978-0-12-088425-4.

Laundal KM, Finlay CC, Olsen N, Reistad JP. 2018. Solar wind and seasonal influence on ionospheric currents from Swarm and CHAMP measurements. *J Geophys Res (Space Phys)* **123(5)**: 4402–4429. https://doi.org/10.1029/2018JA025387.

Lehtinen M, Markkanen J, Väänänen A, Huuskonen A, Damtie B, Nygrén T, Rahkola J. 2002. A new incoherent scatter technique in the EISCAT Svalbard Radar. *Radio Sci* **37(4)**: 1–15. https://doi.org/10.1029/2001RS002518.

Lilensten J, Barthélémy M, Amblard P-O, Lamy H, Wedlund CS, Bommier V, Moen J, Rothkaehl H, Eymard J, Ribot J. 2013. The thermospheric auroral red line polarization: Confirmation of detection and first quantitative analysis. *J Space Weather Space Clim* **3**: A01. https://doi.org/10.1051/swsc/2012023.

Lilensten J, Bommier V, Barthélemy M, Lamy H, Bernard D, Moen JI, Johnsen MG, Løvhaug UP, Pitout F. 2015. The auroral red line polarisation: Modelling and measurements. *J Space Weather Space Clim* **5**: A26. https://doi.org/10.1051/swsc/2015027.

Tanskanen EI. 2009. A comprehensive high-throughput analysis of substorms observed by IMAGE magnetometer network: Years 1993–2003 examined. *J Geophys Res (Space Phys)* **114(A5)**: A05204. https://doi.org/10.1029/2008JA013682.

Thébault E, Finlay CC, Beggan CD, Alken P, Aubert J, et al. 2015. International geomagnetic reference field: The 12th generation. *Earth Planets Space* **67**: 79. https://doi.org/10.1186/s40623-015-0228-9.

Ugolnikov OS, Postylyakov OV, Maslov IA. 2004. Effects of multiple scattering and atmospheric aerosol on the polarization of the twilight sky. *J Quant Spectrosc Radiat Transf* **88**: 233–241. https://doi.org/10.1016/j.jqsrt.2003.12.033.

van de Hulst HC. 1981. *Light scattering by small particles*, Dover Publications, New York. ISBN 978-0-486-64228-4.

Vanhamäki H, Juusola L. 2020. Introduction to spherical elementary current systems. In: *Ionospheric multi-spacecraft analysis tools: Approaches for deriving ionospheric parameters*, Dunlop MW, Lühr H (Eds.), Springer International Publishing, Cham, pp. 5–33. ISBN 978-3-030-26732-2. https://doi.org/10.1007/978-3-030-26732-2_2.

Weygand JM, Amm O, Viljanen A, Angelopoulos V, Murr D, Engebretson MJ, Gleisner H, Mann I. 2011. Application and validation of the spherical elementary currents systems technique for deriving ionospheric equivalent currents with the North American and Greenland ground magnetometer arrays. *J Geophys Res (Space Phys)* **116(A3)**: A03305. https://doi.org/10.1029/2010JA016177.

Witasse O, Lilensten J, Lathuillère C, Blelly PL. 1999. *Modeling the OI 630.0 and 557.7 nm thermospheric dayglow during EISCAT-WINDII coordinated measurements.* **104(A11)**: 24639–24656. https://doi.org/10.1029/1999JA900260.

Appendix A

Error estimation

We present here the S/N parameter described by Bosse et al. (2020) in Appendix A. This parameter is the measure of uncertainty on the polarisation measurements. It is computed from the observed radiant flux (F) in mV, the DoLP (d) in %, and the integration time (T) in ms as:

$$\frac{\mathrm{S}}{\mathrm{N}} = \frac{d}{200}\sqrt{FT}. \tag{A.1}$$

They show that for S/N lower than 4 or 5, the data start to be too noisy for interpretation. Figure A.1 shows the S/N parameter for the raw and smoothed data over the whole observation. The S/N parameter for the raw data ($T = 0.5$ s) is almost always below 4. It can therefore not be interpreted, and the data are not shown in the article for clarity reasons. However, after applying a 20 s smoothing window to the data ($T = 20$ s), the S/N parameter increases to values that allow the interpretation of the data. We can note that this smoothing process averages the signal received over a longer period of time, thus potentially mixing different direction of polarisation together. It corrects the over-evaluation of the DoLP due to noise but might lose information on faster variations. Thus, we make the assumption that the observed polarisation of the aurora does not change during a 20-s interval. As the auroral activity was not too high and the observation spans over hours, this assumption seems reasonable.

During the first half of the observation (before 24 LT), the signal can double over a few minutes, and the S/N parameter is correlated with the radiant flux and the DoLP. It drops to 1 or 2 on a few occasions during a few minutes. During these, the error estimation of the AoLP increases over 180° (see Fig. 3). These portions can not be interpreted, but they do not last very long. In between 24 LT and 25 LT, the S/N parameter is over 5, which corresponds to a period of high DoLP and well-defined AoLP. After 25 h, it drops to zero on two occasions corresponding to the start and end of the 70° jumps described in the article at 25:10 LT and 26:20 LT. The decrease of the S/N parameter during those two jumps is seen in the increase of the AoLP error estimation. However, between the jumps, the S/N parameter is high enough to allow interpretation.

The S/N parameter shows that the data smoothed over 20 s can be used and interpreted over almost the whole observation. Only on a few occasions (during drops in radiant flux and DoLP during the first hour and during the two 70° jumps at 25:10 LT and 26:20 LT.)

Appendix B

Ninox data

We present here the measurements done with the Ninox instrument. The Ninox measures the sky's brightness at the zenith every minute during the observing session. This instrument gathers luminance measurements called NSB for *Night Sky Brightness* and expressed in mag/arcsec^2. Its spectral response essentially covers the visible spectrum (roughly from 320 nm to 720 nm in order to match the human vision), and the FWHM of its field of view is 20°. An NSB of 22.0 mag/arcsec^2 can be achieved under non-polluted and pristine skies (assuming the Milky Way is not in the field of the instrument at the zenith). When passing through the zenith, the Milky Way can account for a decrease of 0.2–0.8 mag/arcsec^2 of the NSB (i.e., sky brightness increases) depending on the galactic longitude. Plots produced with Ninox data are typically smooth under clear skies and erratic in the presence of clouds,

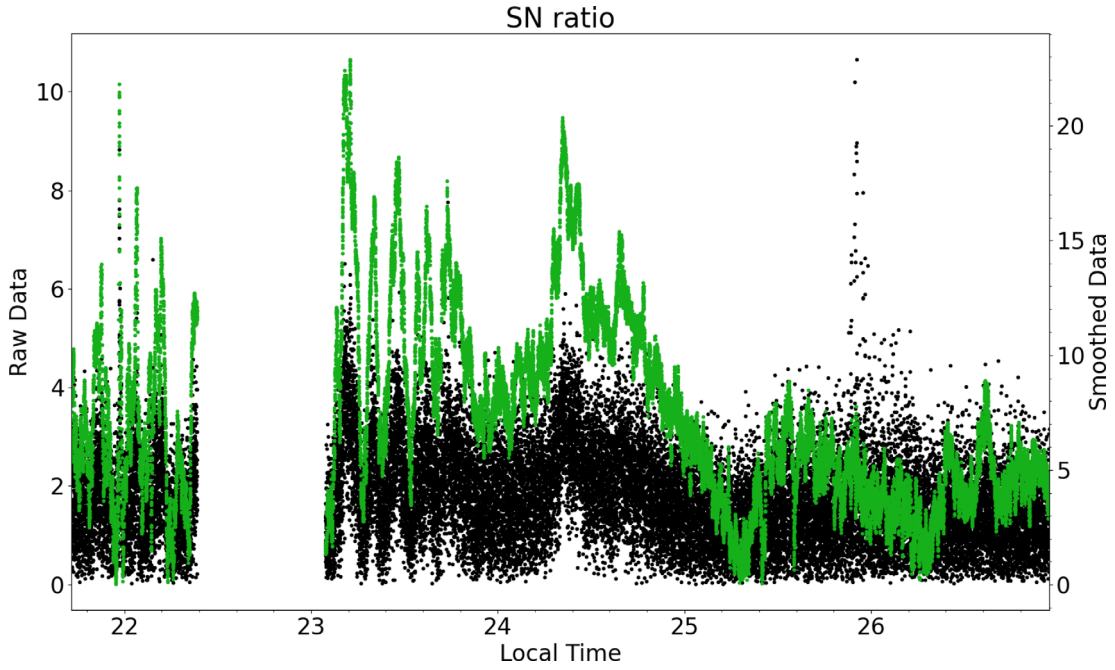

Fig. A.1. S/N parameter over the whole observation, using the method described in Bosse et al. (2020). In black, the values for the raw data (left ordinate) and in green for the smoothed data (right ordinates) over 20 s.

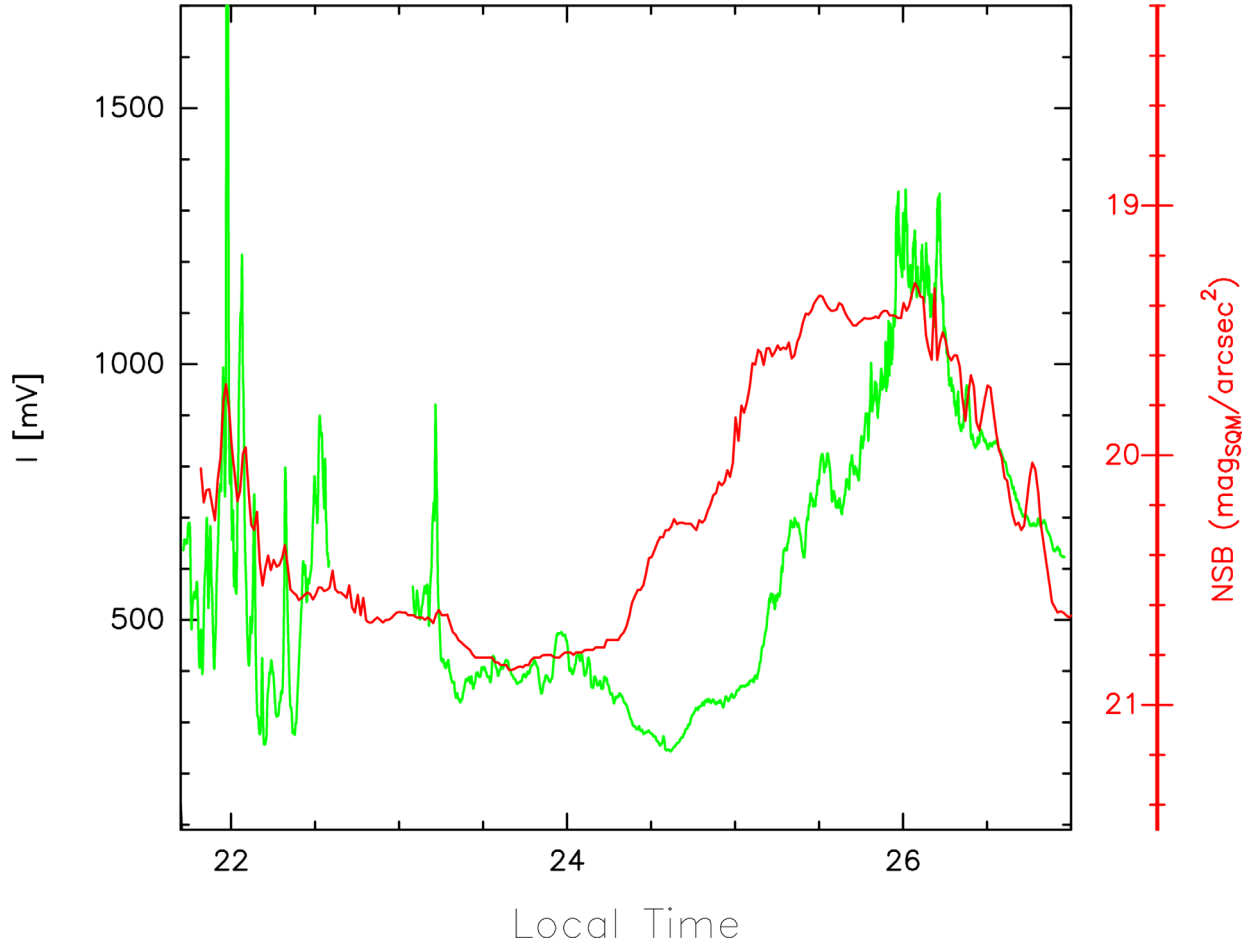

Fig. B.1. This figure compares the Ninox data (in red) to the green line polarimeter radiant flux as in Figure 3 (green line).

especially in sites impacted by light pollution. It was the first time a Ninox was used to measure luminance from auroral emissions, so there were no definitive expectations about the luminance profiles that would be obtained. For this experiment, the Ninox was pointing vertically, i.e., with a 24° pointing difference angle in comparison with the polarimeter.

Figure B.1 shows a comparison between the Ninox and the polarimeter data. Care must be taken to the units which are different, so that only the trend is meaningful (we compare here mV to magnitude per arcsec^2). The global trends are overall comparable. The differences, in particular around 25:00, may be due to the fact that the Ninox integrates over all wavelengths. Indeed, it is sufficient that low energy precipitating electrons create red emissions at 220 km height to increase the Ninox measurements, while the polarimeter only measures the green line at 110 km. Another source of discrepancy lies in the fact that the Ninox was not oriented exactly like the polarimeter but pointed vertically. The third source of difference is the different field of views of the instruments. The polarimeter has a narrower field of view (2°) compared to 20° for the Ninox.

From this comparison, we cannot exclude the possibility that there is a background of light pollution coming from a nearby city. However, this pollution, if any, does not significantly vary overnight and would constitute a background that would hardly disturb this comparison. This assumption is only valid for totally clear sky conditions which was the case during the measurement period reported in Figure B.1.

The red line in Figure B.1, therefore, represents the variation in luminance due to the auoral emissions passing through the zenith. This variation spans over 1.5 magnitude, which is very significant in terms of sky brightness changes. One can notice different dynamics in the luminance changes: some stability around 24:00, low amplitude variations (e.g., just after 22:00), and high amplitude variations (e.g., 26:00). The measured changes in the luminance reflect the radiant flux variations observed with the polarimeter.

Cite this article as: Bosse L, Lilensten J, Johnsen MG, Gillet N, Rochat S, et al. 2022. The polarisation of auroral emissions: A tracer of the E region ionospheric currents. *J. Space Weather Space Clim.* **12**, 17. https://doi.org/10.1051/swsc/2022014.